Molecular Identity Changes of Tumor-Associated Macrophages and Microglia after MRgFUS induced BBB Opening in a Mouse Glioblastoma Model

Yanrong Zhang
Stanford University
Jing Wang
Shandong Provincial Hospital Affiliated to Shandong First Medical University
Sara Ghobadi
Stanford University
Haiyan Zhou
Chengdu University of Traditional Chinese Medicine
Ai Huang
Huazhong University of Science and Technology
Marco Gerosa
University of Verona
Qingyi Hou
Guangdong Provincial People's Hospital
Olivier Keunen
Luxembourg Institute of Health
Anna Golebiewska
Luxembourg Institute of Health
Frezghi G. Habte
Stanford University
Gerald A. Grant
Stanford University School of Medicine
Ramasamy Paulmurugan
Stanford University
Kevin S. Lee
University of Virginia
Max Wintermark (Max.Wintermark@gmail.com)
Stanford University

Research Article

Keywords: Sterile inflammation, Glioblastoma, TAMs, microglia and macrophage activation, Focused Ultrasound, MRgFUS, microbubbles

Posted Date: March 15th, 2022

DOI: https://doi.org/10.21203/rs.3.rs-1437061/v1

Abstract

An orthotopically xenografted mouse GL26 glioma model ($Ccr2^{RFP/wt}$-$Cx3cr1^{GFP/wt}$) was used to evaluate the effect of transient, focal opening of the Blood Brain Barrier (BBB) on the composition of tumor-associated macrophages and microglia (TAMs). Opening of the BBB was induced by Magnetic Resonance Imaging (MRI)-guided focused ultrasound (MRgFUS) combined with systemically-administered microbubbles. CX3CR1-GFP cells and CCR2-RFP cells in brain tumors and in peritumoral tissue were quantified utilizing cell counting in fluroscent, microscopic images. Tumors in animals treated with a single session of MRgFUS did not show significant changes in CX3CR1-GFP or CCR2-RFP cell numbers when compared to tumors in animals not receiving FUS. However, tumors that received two or three sessions of MRgFUS showed significantly increased amounts of both CX3CR1-GFP and CCR2-RFP cells.

The effect of MRgFUS on immune cell compositon of tumors and the brain parenchyma was also characterized and quantified utilizing flow cytometry. Glioma implantation resulted in increased amounts of monocytes, blood-derived macrophages, and microglia-derived macrophages in the brain parenchyma. Tumors administered MRgFUS showed increased numbers of monocytes and blood-derived macrophages. In addition, MRgFUS-treated tumors exhibited more CD80+CD206- cells in monocytes, blood-derived macrophages, microglia, and microglia-derived macrophages, and fewer CD80-CD206+ cells in monocytes and microglia. This signature is indicative of a shift toward a more pro-inflammatory polarization.

In summary, transient, focal opening of the BBB using MRgFUS combined with microbubbles can activate the homing and differentiation of monocytes, and induce a shift towards a more proinflammatory status of the immune environment in glioblastoma.

Background

Glioblastoma (GBM) is the most common and most lethal primary malignancy of the central nervous system. With an incidence of 2–3 per 100,000 population, GBM makes up to 54% of all gliomas and 16% of all primary brain tumors (1). Even with multimodal treatments including surgery, chemotherapy and radiotherapy, the median survival time for patients with GBM is only 14.6 months (2, 3). Despite recent advances in the development of novel therapies against extracranial tumors, very little progress has been made in terms of patient outcome for the treatment of GBM (4). The lack of progress in the development of novel therapies for brain tumors can be attributed, at least in part, to the difficulty of therapeutic agents to cross the blood-brain barrier (BBB) and the dose limited-toxicity that restricts the injection of therapeutic dosages.

The BBB regulates access to the the central nervous system through a tightly regulated neurovascular unit (NVU) including endothelial cells (ECs), pericytes and astrocytic endfeet, which together control the passage of nutrients and metabolites from the blood stream to the brain parenchyma. However, these

same features also hinder the delivery of systemic therapies into brain tumors. While the BBB is often disturbed in brain tumor tissue, the disruption is heterogeneous and only allows smaller molecules to enter, resulting in inadequate drug accumulation in glioblastomas (5) (6). Consequently, the structural and functional heterogeneity of the BBB in the brain tumor microenvironment needs to be considered when attempting to develop effective, systemically-delivered therapies. Multiple strategies are being developed to regulate or disrupt BBB, including the use of osmotic agents (7–9) and the design of molecules utilizing receptor-mediated transport (10).

Transcranial magnetic resonance imaging (MRI)-guided focused ultrasound (MRgFUS), combined with intraveneous microbubbles, has also emerged as an effective strategy for non-invasively opening the BBB (11). MRgFUS oscillates microbubbles and mechanically disrupts the BBB in a targeted, transient, and non-invasive manner, increasing the vascular permeability to large molecules into the brain (12–14). In preclinical studies, MRgFUS-induced opening of the BBB has been used to deliver chemotherapeutic agents (15, 16), antibodies (17, 18), stem cells (19), and therapeutic genes (20). Extensive preclinical research has shown that FUS with microbubbles can lead to a more than 4-fold increase in the delivery and penetration of a range of intravenously administered anticancer agents in brain tumors (21). This improvement in the delivery of anticancer agents has also led to a significant increase in the median survival time (3-fold) in multiple orthotopic murine tumor models, including glioma and breast cancer brain metastasis (22).

Most of the research on MRgFUS-induced BBB opening has focused on using this approach to increase the concentration of therapeutic agents in brain tumors. However, MRgFUS by itself may also directly induce some immune-related responses. Studies on naïve animals have shown that MRgFUS-induced BBB opening elicited sterile inflammation in the normal brain microenvironment. MRgFUS-induced opening of the BBB triggers an acute increase in the transcription of proinflammatory cytokines (23, 24). In intracranial tumor models, MRgFUS combined with microbubbles also has immunomodulatory effects (25). MRgFUS treated gliomas exhibit an increase in the CD8+/T-reg ratio, a metric commonly correlated with improved treatment outcome (26). The immunomodulatory influence of MRgFUS combined with microbubbles on the BBB may thus provide an opportunity for synergy of MRgFUS and immune based therapeutics that could generate a stronger clinical response. A key step in evaluating this intriguing possibility is to investigate how MRgFUS affects the tumor-associated macrophages and microglia (TAMs) in the GBM-TAM pool.

In the current study, we applied MRgFUS together with microbubbles to an immunocompetent mouse glioma model based on orthotopic implantation of GL26 glioma cells. To investigate the composition and functional status of myeloid populations after BBB opening, tumor cells were xenografted to $Ccr2^{RFP/wt}Cx3cr1^{GFP/wt}$ mice carrying genetically color-coded microglia (Cx3cr1-GFP) and blood-derived monocytes and macrophages (Ccr2-RFP). Multistain immunochemistry and flow cytometry (FCM) were utilized to define the changes of TAMs after MRgFUS treatment.

Materials And Methods

Study design

The animal protocol for this study was approved by the Stanford University Administrative Panel on Laboratory Animal Care (APLAC). All experiments were conducted in accordance with the National Institutes of Health's Guide for the Care and Use of Laboratory Animals. Two series of experiments were carried out, one for histological analysis and one for FCM analysis.

Thirty mice with brain tumors were divided into six groups that received the following treatments prior to histology analysis:

- Group 1: No MRgFUS - control group - animals were euthanized when the tumors were 4–5 mm in diameter (n = 5).
- Group 2: MRgFUSx1 - one session of MRgFUS when the tumors were 4mm in diameter and the animals were euthanized 2 days after MRgFUS (n = 5).
- Group 3: MRgFUSx2 - two sessions of MRgFUS every other day starting when the tumors were 3–4 mm in diameter and euthanized at 2 days after the second session of MRgFUS (n = 5).
- Group 4: MRgFUSx3 - three sessions of MRgFUS, once every other day, starting when the tumors were a 2-3mm in diameter, euthanized at 2 days after the last session of MRgFUS (n = 5).

The other ten animals were divided into 2 groups that received the following treatments prior to FCM analysis.

- Group 5: Tumor_No FUS, animals were euthanized when the tumors were 4–5 mm in diameter (n = 5).
- Group 6: Tumor_FUS, three sessions of MRgFUS, once every other day, starting when the tumors were a 2-3mm in diameter, euthanized at 2 days after the last session of MRgFUS (n = 5).

Three naïve animals without brain tumors were euthanized to collect brain tissue for FCM analysis.

Cell Line and Culture

The GL26 mouse glioma cell line was provided by Dr. Ramasamy Paulmurugan and maintained in media consisting of DMEM, 10% FBS, 100ul/ml Penicillin-Streptomycin, and 4mM L-glutamine.

Mice

All mice were housed in specific pathogen-free conditions at a barrier facility at Canary Center at Stanford University School of Medicine (Stanford, California). All animal handling, surveillance, and experimentation was performed in accordance with and approval from the Stanford University Administrative Panel on Laboratory Animal Care.

Homozygous $Ccr2^{RFP/RFP}$ mice (JAX stock #017586) (27) and Cx3cr1-GFP mice (JAX stock #005582) (28) on a C57BL/6 background were purchased from the Jackson Laboratory and intercrossed to yield

$Ccr2^{RFP/wt}Cx3cr1^{GFP/wt}$ animals. To confirm the establishment of heterozygous mice, ear snips were collected when the offspring were 15 through 18 days old, and genotyping was performed using a commercial assay service (Transnetyx, Inc). Previous studies (29) have shown that implantation of murine GL261 glioma cells to the *$Ccr2^{RFP/wt}Cx3cr1^{GFP/wt}$ dual knock–in* mice allowed for efficient evaluation of the myeloid cells, known to constitute the majority of CD45 + immune cells in gliomas. Immunohistochemistry allows for discrimination of CX3CR1-GFP + microglia and TAMs derived thereof and CCR2-RFP + blood-derived monocytes and monocyte-derived TAMs within the tumor as well as in surrounding adjacent brain .

Orthotopic syngeneic model of mouse brain tumors

Mouse glioma GL26 cells dissociated into single-cells suspensions were orthotopically injected into the brain of 8 to 10-week-old *$Ccr2^{RFP/wt}Cx3cr1^{GFP/wt}$* mice using sterotactic injection. In brief, mice were anesthetized with 3% isoflurane (Minrad International, Buffalo, NY, USA) in an induction chamber. Anesthesia on the stereotactic frame (David Kopf Instruments, Tujunga, CA, USA) was maintained with 2% isoflurane/L oxygen delivered through a nose adaptor. A burr hole was placed 1.7 mm lateral and 2 mm posterior of bregma. A blunt-ended needle (75N, 26s/2”/2, 5 µL; Hamilton Co., Reno, NV, USA) was lowered into the burr hole to a depth of 3.5 mm below the dura surface and retracted 0.5 mm to form a small reservoir. Using a microinjection pump (UMP-3; World precision Instruments, Sarasota, FL, USA), $4x10^5$ GL26 cells were injected in a volume of 3 µL at 30 nL/s. After leaving the needle in place for 1 minute, it was retracted at 3 mm/min. The cranial injection site was sealed using biodegradable glue. Tumor formation was followed by MRI using a 3-tesla scanner from MR Solutions. From 1-week post tumor implantation, T2- Fast spin echo (FSE, repetition time/echo time [TR/TE] = 4800/68 ms, flip angle 90°, 2 averages, field of view 28 mm, matrix size = 256x248, slice thickness 1.0 mm) images were acquired once every 2 days to monitor the growth of the tumor. T2*-weighted gradient echo images (repetition time/echo time [TR/TE] = 391/13 ms, flip angle 20°, 3 averages, field of view 28 mm, matrix size = 256x256, slice thickness 1.0 mm) were obtained in order to identify possible hemorrhage.

MRgFUS set up and treatment protocol

MRgFUS was delivered to open the BBB. The MRgFUS system (Image Guided Therapy, Pessac, France) was configured as described in previous studies (30, 31). The system included an MR-compatible, pre-focused, eight-element annular array, 1.5-MHz transducer (spherical radius = 20+/-2 mm, active diameter = 25 mm [focal ratio = 0.8]; Imasonic, Voray sur l’Ognon, France), which was connected to a phased array generator and radiofrequency power amplifier. The transducer and animals were prepared as described in a previous study (32). The membrane in front of the transducer was filled with degassed water and acoustic gel was applied between the transducer and skin. For sonication, the animals were placed in a prone position and maintained in that position using a bite bar and ear bars. The scalp hair was shaved and removed with depilatory cream. The experimental apparatus in this study is shown in Fig. 1.

Definity® Microbubbles (mean diameter range: 1.1–3.3 µm, mean concentration of 1.2×10^{10} bubbles per mL, diluted by 1:20 using 1×PBS, 300 µL/kg, Lantheus Medical Imaging, MA, USA) were injected

through a catheter placed in tail vein just before sonication (1.5 MHz, pulse duration 20-ms, duty cycle of 2%, 1-Hz pulse repetition frequency, 90-s duration per sonication). Multiple sonications were administered in the vicinity of the targeted area of the brain by moving the sonication zones slightly rostro-caudally and medio-laterally targeting the brain tumors. An MR-compatible motorized positioning stage was used to move the transducer in the rostral-caudal and medial-lateral directions. After determining the coordinates of the focal point within the MRI space, treatment planning MRI was acquired, and the focal region was positioned within the tumor. Ultrasound bursts were then applied at peak negative pressure of 0.5MPa.

MRI Data Collection

On the day prior to, and immediately post MRgFUS, a set of MRI data including T2-FSE, T2*-weighted gradient echo, dynamic contrast-enhanced (DCE), and post-contrast T1-weighted images was obtained.

The pre and post-MRgFUS T2-FSE images were acquired in order to assess the size and location of the resulting lesions, T2*-weighted gradient echo images were obtained to identify possible hemorrhagic complications from the MRgFUS procedure. In order to obtain quantitative measurements of BBB permeability, a bolus of gadodiamide contrast (gadobenate dimeglumine; Multihance, Bracco Diagnostics Inc., Monroe Township, NJ 08831, USA) was injected intravenously for DCE imaging (TR/TE = 34/3 ms, average = 1, FOV 28 mm^2, flip angle 20°). Post-contrast T1-weighted imaging (TR/ TE = 620/12 milliseconds, 2 averages, field of view = 28 mm, matrix size = 256x244, slice thickness = 1 mm) was utilized to confirm the opening of the BBB after DCE imaging. Images were reviewed and analyzed using the Horos DICOM viewer. Using FDA-approved commercial software NordicICE (Nordic Neuro Lab, Bergen, Norway), Ktrans maps were computed by using a pipeline inspired by that of Anzalone et al (33). Notably, local AIF adapted for mice studies were extracted from the signal curves using a blind deconvolution method (34).

Tissue Preparation and Analysis

Mice were euthanized with inhalation of 3% isoflurane 2 days after the last MRgFUS session and perfused through the left ventricle at 15 mL/min for 1 min with 0.9% NaCl and then for 30 min with 4% paraformaldehyde in 0.1 M phosphate buffer solution (PBS, pH 7.4). Brains tissues were post-fixed overnight at 4°C and then transferred into 30% (w/v) sucrose in PBS. After equilibrating in the 30% sucrose solution, the brains were sectioned coronally (30 µm) with a sliding microtome. Sections were collected in 30% ethylene glycol and 25% glycerol in 50 mM PBS and stored at 20˚C until used. A 1-in-6 series of sections were collected for nuclear counterstaining with Invitrogen Hoechst 33342 dye. Coronal brain sections containing tumors were acquired with a NanoZoomer Digital Pathology slide scanning system (Hamamatsu Photonics, K.K., Japan).

In order to analyze the histological images, a custom analysis pipeline was setup in order to provide a tool able to quantify in a semi-automated manner the number of GFP and RFP labeled cells per mm^2 on the brain sections. On the images of the stained sections of the brain through Nanozoomer, a Region of

Interest (ROI) was drawn around the brain tumor with the Freehand drawing tool of NDP.view2 software (Hamamatsu Photonics, K.K., Japan) by the the investigators blinded to the identity of the animals and sections they were analyzing. In order to minimize the bias in quantifying the GFP-labeled cells and the RFP-labeled cells, the red and green channel were set both at full dynamic ranges of 200% while the dynamic range of blue channel was switched to 0% and turned off. A simple filter was used to improve the resolution of the image and a magnification factor of 1.8 to 2.5% was applied to the ROIs. Then, the images were exported in .jpg files and analyzed in FIJI (ImageJ). FIJI is an open source software commonly used for biomedical image analysis (35). Upon loading the images in FIJI, the background was first removed using the Rolling Ball Radius algorithm (36, 37). The red and the green channels were then split, and considering the different sizes of the RFP-labeled cells and the GFP-labeled cells, two different radii were adopted to subtract the red and the green components from the background. Otsu thresholding was used on the red and green channel images separately to distinguish positive from negative signals (38, 39). The group above the threshold (automatically computed based on signal intensity in the gray scale) was recognized as the effective signal from the labeled cells and the group below the threshold was recognized as background noise and discarded. The application of a binary mask was followed by the watershed separation as a robust segmentation method, based on the average size of recognized single cells (40). Finally, a simple particle counting method was applied to the resulting images (for the green channel and the red channel) taking into account the average size of the single cells in order to quantify the number of GFP and RFP cells per mm^2. T-test was used to compare the number of GFP and RFP cells per mm^2 from two different groups.

FCM analysis

Mice were deeply anesthetized with 1–4% isofluorane through a nosecone, and transcardially perfused with ice-cold PBS. Brain specimens (left and right brain parenchyma from naïve animals; left and right brain parenchyma, and tumor tissue from the animals with gliomas) were dissected and dissociated into single-cell suspensions using the Brain Tumor Dissociation Kit (Miltenyi Biotech, Catalog # 130-095-942). Cells were then resuspended in ice-cold FCM buffer containing HBSS without Calcium and Magnesium, 2% FBS, and 10mM HEPES. Zombie Nir (Biolegend) staining was applied to exclude dead cells (20 min at 4°C degree), followed by a rinse using an ice-cold FCM buffer. Commercially available rat-anti-mouse CD16/32 antibody (Biolegend) staining for Fc-blocking (20 min at 4°C degree) followed by washing in ice-cold FCM buffer were employed to eliminate nonspecific binding. The cells were then stained with fluorochroma-conjugated antibodies for 30 min at 4°C degree in dark (Table 1), followed by washing in ice-cold FCM buffer. All data were collected on a BD LSR flow cytometer and analyzed using FlowJo 10 software v10.6.1 (Tree Star Inc.).

Two gating strategies were utilized to classify and identify the immune cells in brain and tumor immune microenvironement:

Strategy #1: The cell membrane markers were utilized to classify the immune cells in brain tissues and in brain tumors, TAMs including monocytes, blood-derived macrophages, microglia, and microglia-derived

macrophages were classified from myeloid cells excluding Ly6G + neutrophils. Subsequently, the expressions of CX3CR1-GFP and CCR2-RFP were analyzed from the above four groups (Supplementary figure.1). Gating based on CD80 and CD206 was applied to show the pro-inflammatory (CD80 + CD206-) and anti-inflammatory (CD80-CD206+) polarization of TAMs.

Strategy #2, reverse gating: Genetic gating with CX3CR1-GFP and CCR2-RFP was applied to the myeloid cells, followed by the analysis with Ly6C and F4/80 to identify the subgroups of CX3CR1-GFP and CCR2-RFP expressing cells (Supplementary figure.2).

Results

Confirmation of BBB Opening

On baseline imaging pre-MRgFUS, all 30 tumors showed enhancement, with heterogenous enhancement in 24 tumors and homogenous enhancement in 6 tumors. All of the animals treated with MRgFUS showed enhancement on the postcontrast T1-weighted images in the brain parenchyma along the sonicated area, both in the tumor (more pronounced enhancement than at baseline) and outside the tumor, demonstrating the successful opening of the BBB by MRgFUS. Immediately after sonication, there was no edema on T2-weighted images and no evidence of hemorrhage induced by MRgFUS on T2*-weighted gradient echo images (Fig. 2).

MRgFUS increases infiltration of CX3CR1-GFP and CCR2-RFP cells into the tumor area

GL26 glioma tissues were diffusely infiltrated with CX3CR1-GFP and CCR2-RFP cells in all animals receiving tumors. In the group receiving tumor cell implantation but no FUS (Tumor_No FUS), single-positive CX3CR1-GFP (Fig. 3A, first row, arrows) and CCR2-RFP (Fig. 3A, first row, arrowheads) cells were scattered in the core region of the tumor, and the fluorescent cells were mainly dual-positive cells (Fig. 3A, first row, triangles). There were more CX3CR1-GFP and CCR2-RFP dual-positive cells (Fig. 3A, second row, triangles) at the tumor egde. Single-positive CX3CR1-GFP (Fig. 3A, third row, arrows), CCR2-RFP (Fig. 3A, third row, arrowheads), and dual-positive cells were seen in the peritumoral area, with single-positive CX3CR1-GFP cells seen more frequently seen than CCR2-RFP cells. In the animals that received 3 sessions of MRgFUS (Fig. 3B), there was an substantial increase in CCR2-RFP and CX3CR1-GFP cells. The quantification analysis showed a significant increase in the number of green cells and red cells in the animals treated with 2 and 3 sessions of MRgFUS (Fig. 3C).

Resident microglia are the predominant type of myeloid cells in the untreated brain of the heterozygous animals

CD45 + CD11b + myeloid cells are composed of Ly6G + neutrophils, Ly6G-Ly6C + monocytes, and Ly6G-Ly6C- microglia. Neither Ly6G-Ly6C + F4/80- monocytes, nor Ly6G-Ly6C-F4/80- microglia express F4/80 in naïve brains. More than 97% of the microglia cells are $CX3CR1^{hi}$CCR2- cells (Fig. 4).

Effects of Tumors and MRgFUS on the immune micro-enviroment of parenchymal and tumor tissue

Glioma implantation affected the immune cell composition of the brain parenchyma both ipsilateral and contralateral to the site of the tumor, as compared tissue from the non-implanted brain (Fig. 5A,B). The number of Ly6C + F4/80- monocytes were increased in the brain parenchyma of tumor-bearing brains, with the side of the brain ipsilateral fot the tumor exhibiting a greater increase than the side contralateral to the tumor.

In the dot plots gated from Ly6C and F4/80, Ly6C + F4/80-monocytes also showed a progressive increase across the same categories (arrowheads in Fig. 5B). Figure 5C shows the statistical analysis based on the quantification of the four sub-groups of TAMs gated on Ly6C and F4/80. There was no significant difference in the proportion of monocytes between the naïve brain and contralateral brain parenchyma of animals with implanted gliomas, whereas monocytes increased in the ipsilateral parenchyma around the gliomas. There were more blood-derived macrophages and microglia-derived macrophages in both the contralateral and ipsilateral parenchyma of the animals with brain tumor compared to the naïve brains, the proportion of microglia decreased in the contralateral and ipsilateral brain parenchyma of animals with gliomas compared to the naïve brains. The animals treated with MRgFUS showed increased monocytes (*p = 0.001*) and blood-derived macrophages (*p = 0.01*) compared to the Tumor_No FUS group. Microglia (p = 0.08) and microglia-derived macrophages (p = 0.5) did not show any significant difference between the gliomas from the Tumor_No FUS and Tumor_FUS groups (Fig. 5C).

The plots from the genetic gating strategy from Fig. 5D show that there are more CX3CR1^{hi}CCR2 + differentiated cells, and more newly infiltrated monocytes amongst the CX3CR1^{lo}CCR2 + cells of the gliomas treated with three sessions of MRgFUS. This is consistent with the quantification from the strategy #1.

The quantification analysis showed more CX3CR1^{lo} cells (p = 0.003) and CX3CR1^{hi}CCR2+ (p = 0.003) in the tumors treated with MRgFUS (Fig. 5E).

Effect of MRgFUS on the polarization of TAMs

Figure 6 shows the statistical analysis (t-test) of the CD80 + CD206- and CD80-CD206 + cells. The Tumor_FUS group showed more CD80 + CD206- cells in monocytes (p = 0.04), blood-derived macrophages (p = 0.005), microglia (p = 0.04), and microglia-derived macrophages (p = 0.002) compared to the Tumor_No FUS group. The Tumor_FUS group showed reduced CD80-CD206 + cells in blood-derived macrophages (p = 0.02) and microglia-derived macrophages (p = 0.03) compared to Tumor_No FUS group, the proportion of CD80-CD206 + in monocytes (p = 0.65) and microglia (p = 0.30) did not show significant change between Tumor_FUS and Tumor_No FUS groups.

Discussion

As the most common and aggressive primary brain tumor, GBMs display a high degree of inter- and intra-tumor heterogeneity. The most prevalent non-neoplastic cell population in the GBM microenvironment is comprised of cells of the innate immune system called TAMs, which represent approximately 30–40% of the cells in a GBM (41). These cells have been shown to engage in reciprocal interactions with neoplastic tumor cells to either inhibit or promote tumor growth and progression (42, 43). Efforts have been made to achieve a “re-education” of TAMs by polarizing them toward an M1-like proinflamatory signature from an M2-like anti-inflamatory/tumorigenic signature, with the goal of creating a less supportive tumor microenvironment (44, 45). The purpose of the present study was to evaluate the possibility that treatment with MRgFUS can modify the immune status of the tumor microenvironment in a model of GBM.

As a noninvasive technique that can induce transient BBB opening in targeted brain regions, MRgFUS combined with microbubbles has been shown to successfully deliver large molecules into the brain parenchyma without evidence of micro-hemorrhages (46, 47). This approach has been used to facilitate the delivery of drugs and genes to treat stroke, neurodegenerative disease, and primary and metastatic brain tumors in animal models (48–51). In addition, MRgFUS by itself may directly exert certain immune-related effects. In studies of normal brain, MRgFUS combined with microbubbles induces microglia activation (23, 52, 53), and elicits macrophage homing from the periphery to sonicated regions of the brain (23). Studies using mouse models of Alzheimer’s disease have shown that repeated MRgFUS treatments lead to a 20% reduction in Amyloid-β plaque load (51, 54), effects that may be the result of MRgFUS-induced increases in endogenous immunoglobulins, activated microglia, and activated astrocytes. Although sterile inflammation, microglial activation, and macrophage homing produced by MRgFUS have been well studied, there is little known about how MRgFUS impacts the cellular phenotypes of TAMs.

In our study, histological assessments did not demonstrate significant changes in the CX3CR1- GFP or CCR2-RFP cells in tumors that received only one session of MRgFUS. However, tumors that received two or three sessions of MRgFUS showed increased numbers of CX3CR1-GFP cells and CCR2-RFP cells, with the animals receiving three sessions exhibiting the most abundant increases. One limitation of using histological quantification of cellular phenotypes is the difficulty in defining the number of dual-positive cells, which form the predominant population of TAMs. Consequently, in order to distinguish among the CX3CR1-GFP, CCR2-RFP, and CX3CR1-GFP/CCR2-RFP dual positive cells in the TAMs pool, FCM was used to analyze the immune cells in naïve brain parenchyma, brain parenchyma ipsilateral and contralateral to a tumor, and in brain tumors that did or did not receive MRgFUS treatment. In naïve brains, almost all of the myeloid cells were Ly6G-Ly6C- microglia, and these cells were almost exclisively CX3CR1^{hi}CCR2-. Implantation of GL26 glioma cells into the brain significantly modified the immune environment of the brain parenchyma. Contralateral to the tumor, monocyte numbers were not changed significantly. However, differentiated cells, including blood-derived macrophages and microglia-derived macrophages were increased, while the proportion of microglia was decreased. In the brain parenchyma ipsilateral to

the tumor, blood- and microglia-derived macrophages were increased, while the proportion of the microglia was decreased.

Based on the expression of traditional cell surface markers (CD45, CD11b, Ly/6G, Ly6C, F4/80), FCM findings demonstrated an increase in monocytes and blood-derived macrophages in tumors treated with MRgFUS, which is consistent with findings from previous studies showing that MRgFUS causes macrophages to home to a sonicated region (23). Based on genetic markers, FCM discriminated between the single-positive CX3CR1-GFP, CCR2-RFP, and dual-positive CD3CR1-GFP/CCR2-RFP cells, and these cells expressed different levels of CXCR1-GFP. The tumors treated with MRgFUS showed more $CX3CR1^{hi}CCR2+$ cells which mainly represent differentiated TAMS from both monocytes and microglia. Treated tumors also contained more newly infiltrated monocytes, gated on Ly6C and F4/80 from $CX3CR1^{lo}CCR2+$ cells. These findings indicate that MRgFUS induces homing of monocytes and promotes differentiation of TAMs.

Under physiological conditions, immune cells in naïve brains do not show pro-inflammatory or anti-inflammatory phenotypes, based on the lack of CD80 + CD206- or CD80-CD206 + cells. The animals from the Tumor_FUS group showed more CD80 + CD206- cells in monocytes, blood-derived macrophages, microglia, and microglia-derived macrophages, while the number of blood- and microglia-derived macrophages that were CD80-CD206 + was reduced. This indicates that MRgFUS induces monocytes, blood-derived macrophages, microglia and microglia-derived macrophages in the direction of pro-inflammatory polarization. This may be the result of the increased expression of cytokines after MRgFUS. Previous evidence of MRgFUS-induced sterile inflammation in normal brain (23) has shown an immediate increase in multiple cytokines including TNFα, IL1α, IL1β, and IL18. These changes could in turn induce an increase in chemotactic factors for immune cells (MCP1, G-CSF, GM-CSF, MIP3α, and RANTES), among which IL1β and TNFα are pro-inflammatory cytokines.

Conclusion

Treatment of tumors with MRgFUS combined with microbubbles promotes the homing and differentiation of monocytes and induces the polarization of monocytes, macrophages, and microglia in a pro-inflammatory direction. This non-invasive procedure therefore holds promise for future development both as a stand-alone therapeutic strategy, as well an adjunct strategy for facilitating the delivery of chemotheraputic agents for the treatment of GBM.

Abbreviations

BBB: Blood Brain Barrier

TAMs: Tumor-associated macrophages and microglia

MRI: Magnetic Resonance Imaging

MRgFUS: Magnetic Resonance Imaging-guided focused ultrasound

CX3CR1: CX3C chemokine receptor 1

CCR2: C-C chemokine receptor type 2

GFP: Green fluorescent protein

RFP: Red fluorescent protein

WT: Wild type

CD45: Protein tyrosine phosphatase receptor type C (PTPRC)

CD11b: Integrin alpha M (ITGAM)

F4/80: EGF-like module-containing mucin-like hormone receptor-like 1 (EMR1)

Ly6C: Lymphocyte antigen 6C

Ly6G: Lymphocyte antigen 6 complex locus G6D

CD80: Cluster of differentiation 80

CD206: Cluster of Differentiation 206

GBM: Glioblastoma

NVU: neurovascular unit

ECs: Endothelial cells

FCM: Flow cytometry

APLAC: Administrative Panel on Laboratory Animal Care

TR/TE: Repetition time/echo time

FSE: Fast spin echo

DCE: Dynamic contrast-enhanced

GRE: Gradient echo image

PBS: Phosphate buffer solution

ROI: Region of Interest

TNFα: Tumor necrosis factor alpha

IL1α: Interleukin 1 alpha

IL1β: Interleukin 1 beta

IL18: Interleukin-18

MCP1: Monocyte chemoattractant protein-1

G-CSF: Granulocyte colony stimulating factor

GM-CSF: Granulocyte macrophage-colony stimulating factor

MIP3α: Macrophage Inflammatory Protein-3α

RANTES: Regulated upon Activation, Normal T Cell Expressed and Presumably Secreted

Declarations

Availability of data

The datasets used and/or analysed during the current study are available from the corresponding author on reasonable request.

Ethics approval and consent to participate

Animal experimentation was approved by the Stanford University Administrative Panel on Laboratory Animal Care (APLAC). All experiments were conducted in accordance with the National Institutes of Health's Guide for the Care and Use of Laboratory Animals.

Consent for publication

Not applicable.

Competing interests

The authors declare that they have no competing interests.

Funding

This work was supported by National Institutes of Health Grants R01 CA217953-01 and R01 NS102194.

Authors' contributions

Conception and design: Lee, Wintermark. Animal model: Ghobadi, Zhou. MRI technical support: Keunen, Habte. Acquisition of data: Zhang, Wang, Ghobadi, Zhou, Huang, Hou, Keunen. Analysis and

interpretation of data: Zhang, Gerosa, Keunen, Golebiewska. Drafting the article: Zhang. Critically revising the article: Zhang, Keunen, Golebiewska, Paulmurugan, Lee, Wintermark. Reviewed submitted version of manuscript: Zhang, Grant, Paulmurugan, Lee,Wintermark. Approved the final version of the manuscript on behalf of all authors: Wintermark.

References

1. Ostrom QT, Patil N, Cioffi G, Waite K, Kruchko C, Barnholtz-Sloan JS. CBTRUS Statistical Report: Primary Brain and Other Central Nervous System Tumors Diagnosed in the United States in 2013–2017. Neuro Oncol. 2020;22(12 Suppl 2):iv1-iv96.
2. Thakkar JP, Dolecek TA, Horbinski C, Ostrom QT, Lightner DD, Barnholtz-Sloan JS, et al. Epidemiologic and molecular prognostic review of glioblastoma. Cancer Epidemiol Biomarkers Prev. 2014;23(10):1985–96.
3. Louis DN, Perry A, Wesseling P, Brat DJ, Cree IA, Figarella-Branger D, et al. The 2021 WHO Classification of Tumors of the Central Nervous System: a summary. Neuro Oncol. 2021;23(8):1231–51.
4. Maxwell R, Jackson CM, Lim M. Clinical Trials Investigating Immune Checkpoint Blockade in Glioblastoma. Curr Treat Options Oncol. 2017;18(8):51.
5. Sarkaria JN, Hu LS, Parney IF, Pafundi DH, Brinkmann DH, Laack NN, et al. Is the blood-brain barrier really disrupted in all glioblastomas? A critical assessment of existing clinical data. Neuro Oncol. 2018;20(2):184–91.
6. Zhou W, Chen C, Shi Y, Wu Q, Gimple RC, Fang X, et al. Targeting Glioma Stem Cell-Derived Pericytes Disrupts the Blood-Tumor Barrier and Improves Chemotherapeutic Efficacy. Cell Stem Cell. 2017;21(5):591–603 e4.
7. Rodriguez A, Tatter SB, Debinski W. Neurosurgical Techniques for Disruption of the Blood-Brain Barrier for Glioblastoma Treatment. Pharmaceutics. 2015;7(3):175–87.
8. Gumerlock MK, Belshe BD, Madsen R, Watts C. Osmotic blood-brain barrier disruption and chemotherapy in the treatment of high grade malignant glioma: patient series and literature review. J Neurooncol. 1992;12(1):33–46.
9. Duskey JT, Belletti D, Pederzoli F, Vandelli MA, Forni F, Ruozi B, et al. Current Strategies for the Delivery of Therapeutic Proteins and Enzymes to Treat Brain Disorders. Int Rev Neurobiol. 2017;137:1–28.
10. Lajoie JM, Shusta EV. Targeting receptor-mediated transport for delivery of biologics across the blood-brain barrier. Annu Rev Pharmacol Toxicol. 2015;55:613–31.
11. Jolesz FA, McDannold NJ. Magnetic resonance-guided focused ultrasound: a new technology for clinical neurosciences. Neurol Clin. 2014;32(1):253–69.
12. Fry FJ, Ades HW, Fry WJ. Production of reversible changes in the central nervous system by ultrasound. Science. 1958;127(3289):83–4.

13. Fry WJ. Intense ultrasound in investigations of the central nervous system. Adv Biol Med Phys. 1958;6:281–348.
14. Hynynen K, McDannold N, Vykhodtseva N, Jolesz FA. Non-invasive opening of BBB by focused ultrasound. Acta Neurochir Suppl. 2003;86:555–8.
15. Treat LH, McDannold N, Zhang Y, Vykhodtseva N, Hynynen K. Improved anti-tumor effect of liposomal doxorubicin after targeted blood-brain barrier disruption by MRI-guided focused ultrasound in rat glioma. Ultrasound Med Biol. 2012;38(10):1716–25.
16. Mainprize T, Lipsman N, Huang Y, Meng Y, Bethune A, Ironside S, et al. Blood-Brain Barrier Opening in Primary Brain Tumors with Non-invasive MR-Guided Focused Ultrasound: A Clinical Safety and Feasibility Study. Sci Rep. 2019;9(1):321.
17. Kinoshita M, McDannold N, Jolesz FA, Hynynen K. Targeted delivery of antibodies through the blood-brain barrier by MRI-guided focused ultrasound. Biochem Biophys Res Commun. 2006;340(4):1085–90.
18. Jordao JF, Ayala-Grosso CA, Markham K, Huang Y, Chopra R, McLaurin J, et al. Antibodies targeted to the brain with image-guided focused ultrasound reduces amyloid-beta plaque load in the TgCRND8 mouse model of Alzheimer's disease. PLoS One. 2010;5(5):e10549.
19. Burgess A, Ayala-Grosso CA, Ganguly M, Jordao JF, Aubert I, Hynynen K. Targeted delivery of neural stem cells to the brain using MRI-guided focused ultrasound to disrupt the blood-brain barrier. PLoS One. 2011;6(11):e27877.
20. Noroozian Z, Xhima K, Huang Y, Kaspar BK, Kugler S, Hynynen K, et al. MRI-Guided Focused Ultrasound for Targeted Delivery of rAAV to the Brain. Methods Mol Biol. 2019;1950:177–97.
21. Aryal M, Arvanitis CD, Alexander PM, McDannold N. Ultrasound-mediated blood-brain barrier disruption for targeted drug delivery in the central nervous system. Adv Drug Deliv Rev. 2014;72:94–109.
22. Arvanitis CD, Askoxylakis V, Guo Y, Datta M, Kloepper J, Ferraro GB, et al. Mechanisms of enhanced drug delivery in brain metastases with focused ultrasound-induced blood-tumor barrier disruption. Proc Natl Acad Sci U S A. 2018;115(37):E8717-E26.
23. Kovacs ZI, Kim S, Jikaria N, Qureshi F, Milo B, Lewis BK, et al. Disrupting the blood-brain barrier by focused ultrasound induces sterile inflammation. Proc Natl Acad Sci U S A. 2017;114(1):E75-E84.
24. McMahon D, Bendayan R, Hynynen K. Acute effects of focused ultrasound-induced increases in blood-brain barrier permeability on rat microvascular transcriptome. Sci Rep. 2017;7:45657.
25. Chen H, Hou GY, Han Y, Payen T, Palermo CF, Olive KP, et al. Harmonic motion imaging for abdominal tumor detection and high-intensity focused ultrasound ablation monitoring: an in vivo feasibility study in a transgenic mouse model of pancreatic cancer. IEEE Trans Ultrason Ferroelectr Freq Control. 2015;62(9):1662–73.
26. Chen PY, Hsieh HY, Huang CY, Lin CY, Wei KC, Liu HL. Focused ultrasound-induced blood-brain barrier opening to enhance interleukin-12 delivery for brain tumor immunotherapy: a preclinical feasibility study. J Transl Med. 2015;13:93.

27. Saederup N, Cardona AE, Croft K, Mizutani M, Cotleur AC, Tsou CL, et al. Selective chemokine receptor usage by central nervous system myeloid cells in CCR2-red fluorescent protein knock-in mice. PLoS One. 2010;5(10):e13693.
28. Jung S, Aliberti J, Graemmel P, Sunshine MJ, Kreutzberg GW, Sher A, et al. Analysis of fractalkine receptor CX(3)CR1 function by targeted deletion and green fluorescent protein reporter gene insertion. Mol Cell Biol. 2000;20(11):4106–14.
29. Chen Z, Feng X, Herting CJ, Garcia VA, Nie K, Pong WW, et al. Cellular and Molecular Identity of Tumor-Associated Macrophages in Glioblastoma. Cancer Res. 2017;77(9):2266–78.
30. Zhang Y, Aubry JF, Zhang J, Wang Y, Roy J, Mata JF, et al. Defining the optimal age for focal lesioning in a rat model of transcranial HIFU. Ultrasound Med Biol. 2015;41(2):449–55.
31. Zhang Y, Tan H, Bertram EH, Aubry JF, Lopes MB, Roy J, et al. Non-Invasive, Focal Disconnection of Brain Circuitry Using Magnetic Resonance-Guided Low-Intensity Focused Ultrasound to Deliver a Neurotoxin. Ultrasound Med Biol. 2016;42(9):2261–9.
32. Zhang Y, Zhou H, Qu H, Liao C, Jiang H, Huang S, et al. Effects of Non-invasive, Targeted, Neuronal Lesions on Seizures in a Mouse Model of Temporal Lobe Epilepsy. Ultrasound Med Biol. 2020;46(5):1224–34.
33. Anzalone N, Castellano A, Cadioli M, Conte GM, Cuccarini V, Bizzi A, et al. Brain Gliomas: Multicenter Standardized Assessment of Dynamic Contrast-enhanced and Dynamic Susceptibility Contrast MR Images. Radiology. 2018;287(3):933–43.
34. Jirik R, Taxt T, Macicek O, Bartos M, Kratochvila J, Soucek K, et al. Blind deconvolution estimation of an arterial input function for small animal DCE-MRI. Magn Reson Imaging. 2019;62:46–56.
35. Schindelin J, Arganda-Carreras I, Frise E, Kaynig V, Longair M, Pietzsch T, et al. Fiji: an open-source platform for biological-image analysis. Nat Methods. 2012;9(7):676–82.
36. Kuwahara M, Eiho S. [Image processing technics–focus on software. 1. Perspectives in biomedical image processing]. Iyodenshi To Seitai Kogaku. 1983;21(4):266–73.
37. Sternberg R. S. Biomedical Image Processing. IEEE Computer. 1983;16:22–34.
38. Hetal J. Vala AB. A review on Otsu image segmentation algorithm.. International Journal of Advanced Research in Computer Engineering and Technology. 2013;2(2):387–9.
39. Hetal J. Vala AB. A review on Otsu image segmentation algorithm.. International Journal of Advanced Research in Computer Engineering and Technology 2013;2(2):387–9.
40. Ankit Chadha NS. A Robust Approach to Image Segmentation with Optimal Thresholding and Watershed Transform. International Journal of Computer Applications. 2013;65(9):1–7.
41. Charles NA, Holland EC, Gilbertson R, Glass R, Kettenmann H. The brain tumor microenvironment. Glia. 2012;60(3):502–14.
42. Feng X, Szulzewsky F, Yerevanian A, Chen Z, Heinzmann D, Rasmussen RD, et al. Loss of CX3CR1 increases accumulation of inflammatory monocytes and promotes gliomagenesis. Oncotarget. 2015;6(17):15077–94.

43. Hu F, Dzaye O, Hahn A, Yu Y, Scavetta RJ, Dittmar G, et al. Glioma-derived versican promotes tumor expansion via glioma-associated microglial/macrophages Toll-like receptor 2 signaling. Neuro Oncol. 2015;17(2):200–10.
44. Wang Y, Lin YX, Qiao SL, An HW, Ma Y, Qiao ZY, et al. Polymeric nanoparticles promote macrophage reversal from M2 to M1 phenotypes in the tumor microenvironment. Biomaterials. 2017;112:153–63.
45. Chen Z, Hambardzumyan D. Immune Microenvironment in Glioblastoma Subtypes. Front Immunol. 2018;9:1004.
46. Tung YS, Vlachos F, Choi JJ, Deffieux T, Selert K, Konofagou EE. In vivo transcranial cavitation threshold detection during ultrasound-induced blood-brain barrier opening in mice. Phys Med Biol. 2010;55(20):6141–55.
47. Hynynen K, McDannold N, Vykhodtseva N, Jolesz FA. Noninvasive MR imaging-guided focal opening of the blood-brain barrier in rabbits. Radiology. 2001;220(3):640–6.
48. Leinenga G, Langton C, Nisbet R, Gotz J. Ultrasound treatment of neurological diseases–current and emerging applications. Nat Rev Neurol. 2016;12(3):161–74.
49. Burgess A, Hynynen K. Drug delivery across the blood-brain barrier using focused ultrasound. Expert Opin Drug Deliv. 2014;11(5):711–21.
50. Kovacs Z, Werner B, Rassi A, Sass JO, Martin-Fiori E, Bernasconi M. Prolonged survival upon ultrasound-enhanced doxorubicin delivery in two syngenic glioblastoma mouse models. J Control Release. 2014;187:74–82.
51. Burgess A, Dubey S, Yeung S, Hough O, Eterman N, Aubert I, et al. Alzheimer disease in a mouse model: MR imaging-guided focused ultrasound targeted to the hippocampus opens the blood-brain barrier and improves pathologic abnormalities and behavior. Radiology. 2014;273(3):736–45.
52. Alonso A, Reinz E, Fatar M, Hennerici MG, Meairs S. Clearance of albumin following ultrasound-induced blood-brain barrier opening is mediated by glial but not neuronal cells. Brain Res. 2011;1411:9–16.
53. Sinharay S, Tu TW, Kovacs ZI, Schreiber-Stainthorp W, Sundby M, Zhang X, et al. In vivo imaging of sterile microglial activation in rat brain after disrupting the blood-brain barrier with pulsed focused ultrasound: [18F]DPA-714 PET study. J Neuroinflammation. 2019;16(1):155.
54. Jordao JF, Thevenot E, Markham-Coultes K, Scarcelli T, Weng YQ, Xhima K, et al. Amyloid-beta plaque reduction, endogenous antibody delivery and glial activation by brain-targeted, transcranial focused ultrasound. Exp Neurol. 2013;248:16–29.

Tables

Table1. Antibodies used in flowcytometry analysis

Epitope	Conjugate	Clone	Concentration (ul/test)	Supplier	Laser	Filter
CD45	Brilliant Violet 605	30-F11	1.5	BD Biosciences	Vio-3 (610/20)	QD605, BV605
CD11b	PerCP/Cy5.5	M1/70	5	BioLegend	488nm Blue	B2 (710/50)/ 550LP
Ly6G	Brilliant Violet 785	1A8	2.5	BioLegend	405nm Violet	Vio-6 (780/60)
Ly6C	Pacific blue	HK1.4	0.5	BioLegend	405nm Violet	Vio-1 (450/50)
F4/80	Brilliant Ultraviolet 395	T45-2342	1	BD Biosciences	355nm UV	UV-1 (379/29)
CD206	APC	C068C2	2.5	BioLegend	640nm Red	Red1 (670/30)
CD80	Brilliant Ultraviolet 737	16-10A1	2	BD Biosciences	355nm UV	UV-1 (740/30)

Figures

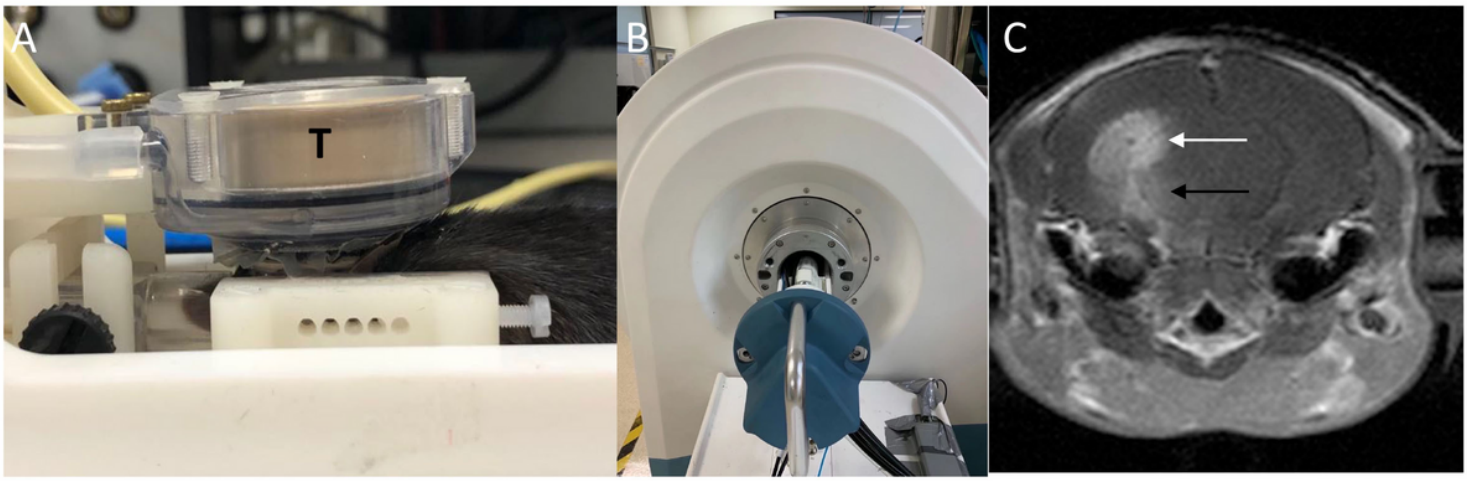

Figure 1

Experimental apparatus and post contrast T1-weighted image immediately after sonication. A: MRgFUS system consisting of a 1.5-MHz transducer (T) that rests on the top of the mouse head and can move in X-Y planes and can be focused in the Z axis. B: A 3T MRI scanner was used to detect BBB-opening after sonication. C: Post-contrast T1-weighted image acquired immediately after sonication. Enhancement of the tumor (white arrow) and the brain tissue along the acoustic beam below the tumor (black arrow) indicates the area of BBB opening.

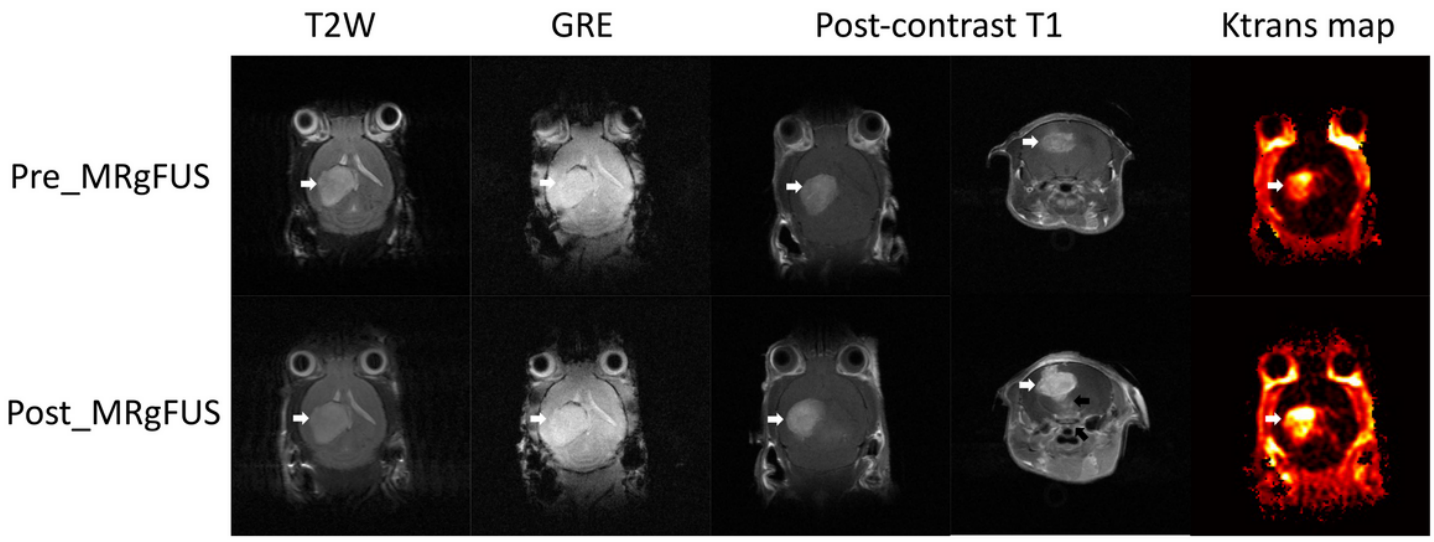

Figure 2

Examples of MR images of GL26 xenograft acquired before and immediately post MRgFUS. T2-weighted images did not show edema after MRgFUS. T2*-weighted gradient echo image (GRE) did not show hemorrhage from MRgFUS. Post-contrast T1-weighted images showed the enhancement of the tumor both before and post MRgFUS (white arrows), with a more pronounced enhancement on the post MRgFUS images. Post-contrast T1-weighted images in the axial plane also showed the enhancement in the brain tissue below the tumor along the path of the ultrasound beam (black arrow). Ktrans map from horizontal direction showed elevated Ktrans in the tumor prior to MRgFUS and an increase in Ktrans signal upon MRgFUS induction (white arrows).

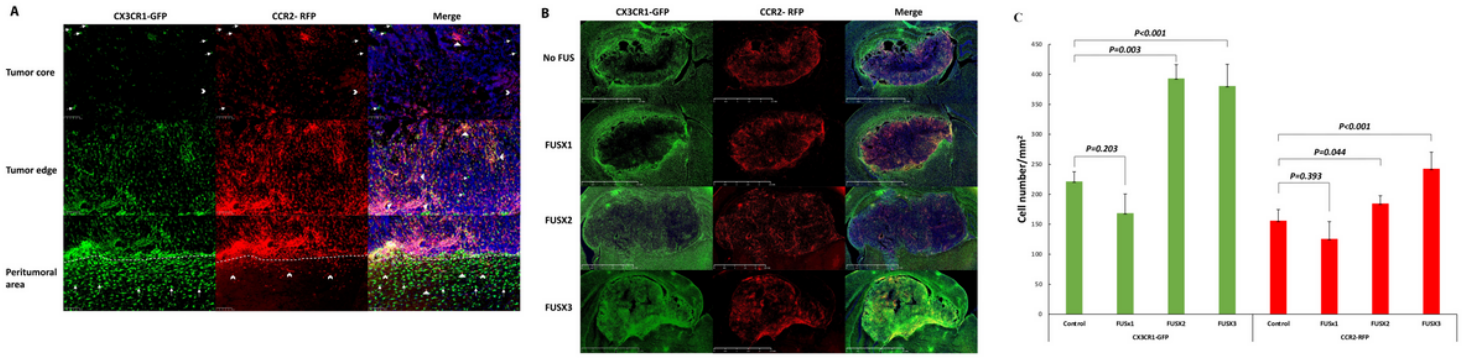

Figure 3

Infiltration of brain tumors by CCR2-RFP and CX3CR1-GFP immune cells.

A) Immunohistochemical staining for CX3CR1-GFP and CCR2-RFP cells is shown from an animal in the tumor-implanted group that did not receive MRgFUS. The fluorescent immune cells are mainly located at the edges of the tumor and in the peritumoral area with only a sparse distribution of cells in the core. Both in the tumor core and at the edges, dual-positive cells (First and second rows, triangles) are the

predominant type, with occasional single-positive CX3CR1-GFP (First row, arrows) and CCR2-RFP (First and second rows, arrow heads) cells. In the peritumoral area (i.e. the areas below the dotted lines in the lower panels), there are more single-positive CX3CR1-GFP cells than single-positive CCR2-RFP cells, although dual-positive cells are seen in this area as well. B) Lower magnification images encompassing the tumor and peritumoral area for four experimental groups are shown. As described in A, stained cells in the Tumor_No FUS group exhibit stained cells toward the periphery of the tumor and in the peritumoral area. One session of FUS (FUSX1) did not appear to alter the distribution of cells. In contrast, two or three sessions of FUS (FUSX2 and FUSX3, respectively) resulted in increased numbers of immune cells infiltrating the tumor. C) Quantification of the cell density across the core and periphery of tumors demonstrated significantly greater infiltration of immune cells into tumors in animals receiving 2 or 3 sessions of FUS. Values shown are means and standard errors. T-test was used to compare the values between different groups.

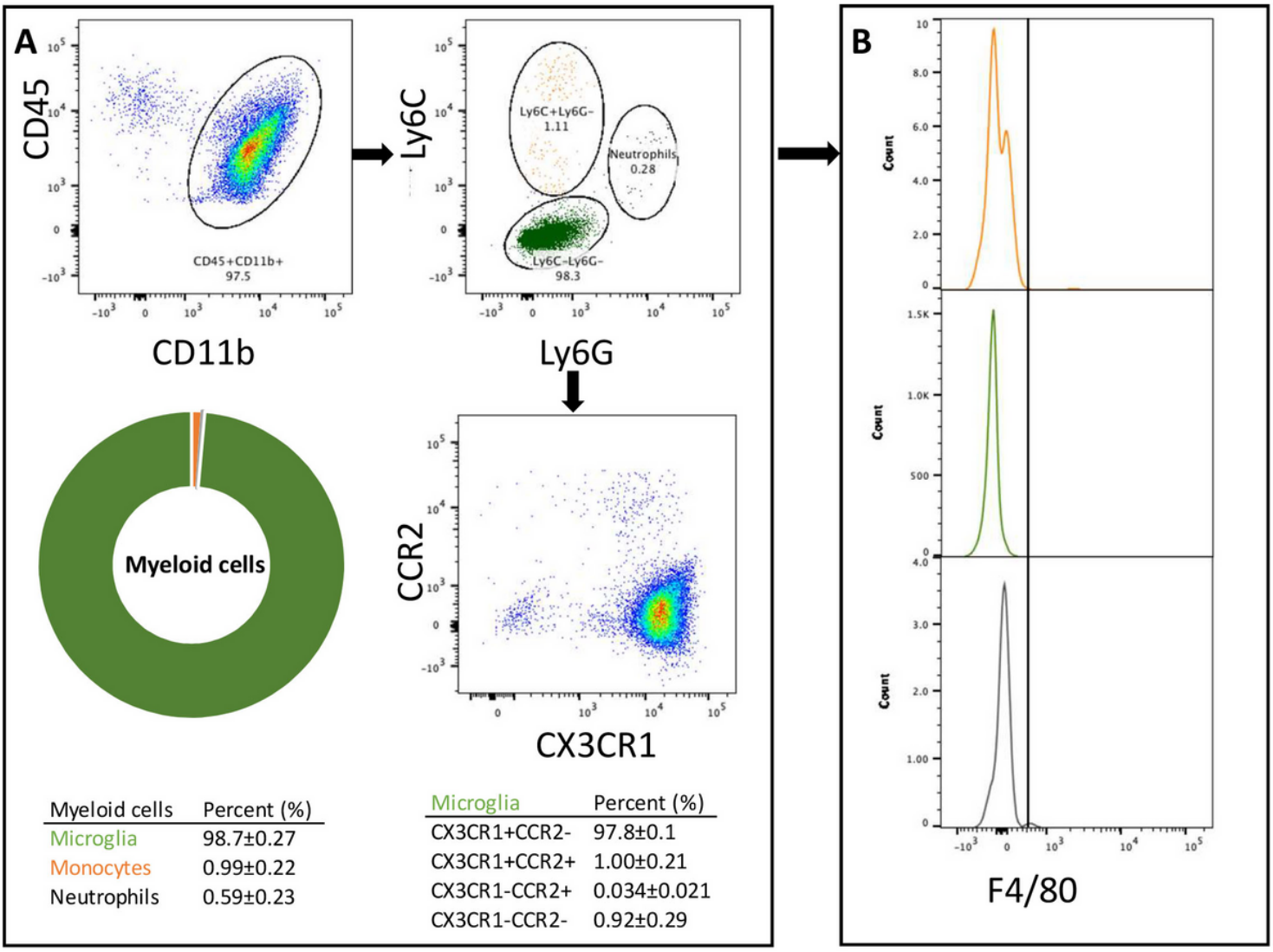

Myeloid cells	Percent (%)
Microglia	98.7±0.27
Monocytes	0.99±0.22
Neutrophils	0.59±0.23

Microglia	Percent (%)
CX3CR1+CCR2-	97.8±0.1
CX3CR1+CCR2+	1.00±0.21
CX3CR1-CCR2+	0.034±0.021
CX3CR1-CCR2-	0.92±0.29

Figure 4

Resident microglia are the predominant type of myeloid cells in the untreated brain of the heterozygous animals. A) The predominant type of the myeloid cells in the untreated brain are Ly6G-Ly6C- microglia. In microglia, 97±0.1% of the cells are CX3CR1+CCR2- with CX3CR1-GFP expression higher than 10^4. B) None of the three subgroups of myeloid cells, including Ly6G+ neutrophils, Ly6G-Ly6C+ monocytes, and Ly6G-Ly6C- microglia, express F4/80, which indicates that monocytes and resident microglia are undifferentiated under physiological status.

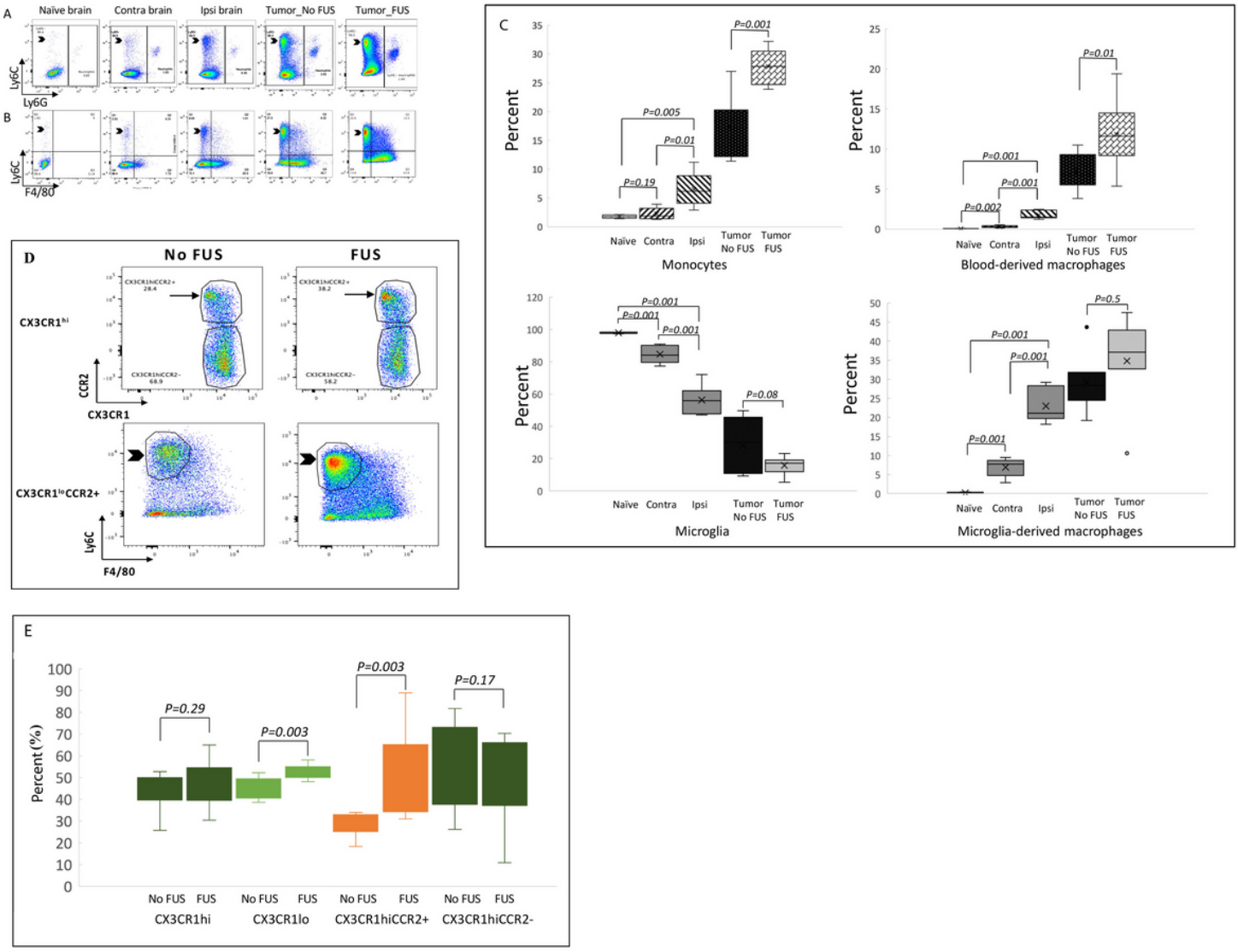

Figure 5

Effects of Tumors and MRgFUS on the immune micro-enviroment of parenchymal and tumor tissue. A) Dot plots gated from strategy #1 showed increased Ly6G-Ly6C+ monocytes (arrowheads) in the parenchyma of tumor-implanted brains. Higher numbers of LY6G-LY6C+ were observed in tumor tissue and MRgFUS treatment of the tumor further increased the numbers of these cells. increase. B) Plots gated from strategy #1 showed increased Ly6C+F4/80- monocytes and Ly6C+F4/80+ blood-derived

macrophages in the parenchyma of tumor-implanted brains tumors. Higher numbers of Ly6C+F4/80- in tumor tissue and MRgFUS treatment of the tumor further increased the numbers of these cells. Microglia (Ly6C-F4/80-) and microglia-derived macrophages (Ly6C-F4/80+) did not show significant different between Tumor_No FUS and Tumor_FUS groups. C) There was no significant difference in the proportion of monocytes comparing the naïve brain and contralateral parenchyma of animals with tumor implanted (p=0.19), whereas monocytes increased in the ipsilateral parenchyma (p=0.005). There were more blood-derived macrophages and microglia-derived macrophages in the contralateral and ipsilateral parenchyma of animals with brain tumor compared to naïve brains. The proportion of resident microglia decreased in the contralateral and ipsilateral parenchyma of animals with brain tumor compared to naïve brains. Three sessions of FUS induced accumulation of monocytes (P=0.001) and blood-derived macrophages (p=0.01); however, microglia (p=0.08) and microglia-derived macrophages (p=0.5) did not show statistical difference between the tumors of control and MRgFUS groups. D) The dot plots from the genetic gating strategy showed that MRgFUS induced more CX3CR1^{hi}CCR2+ cells (arrows), representing differentiated cells, and more Ly6C+F4/80- monocytes (arrowheads) from CX3CR1^{lo}CCR2+ cells. E) The quantification analysis showed more CX3CR1^{lo} cells (p=0.003) and CX3CR1^{hi}CCR2+ (p=0.003) in the tumors treated with MRgFUS. Abbreviation: contra: contralateral parenchyma; Ipsi: ipsilateral parenchyma.

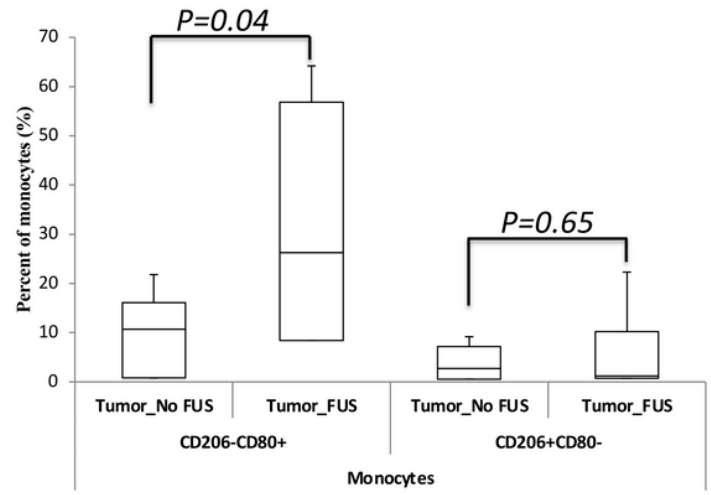

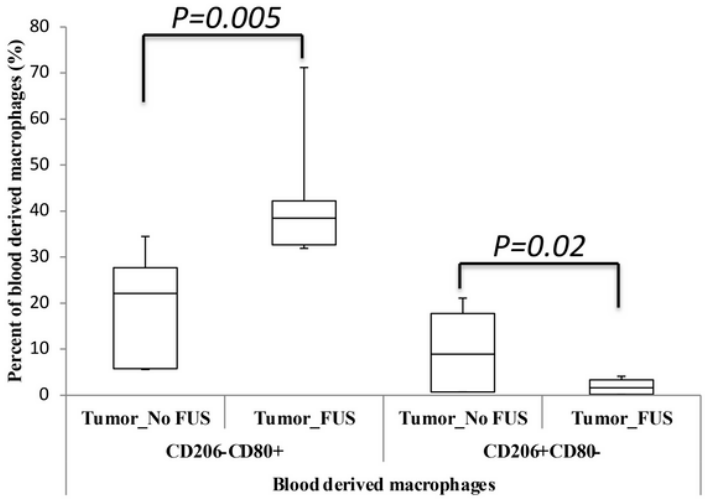

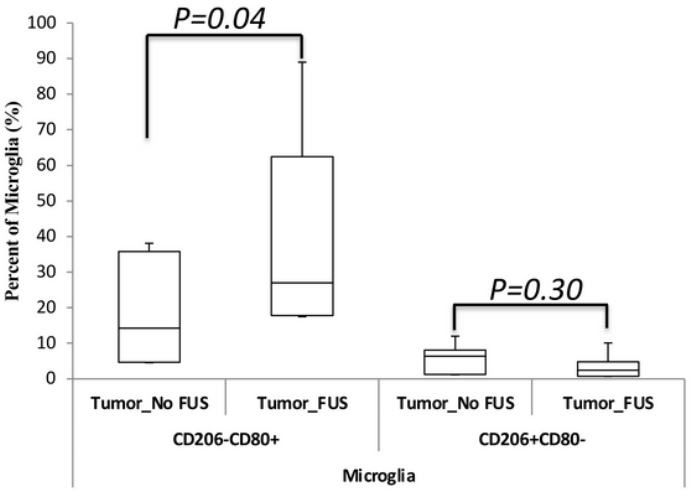

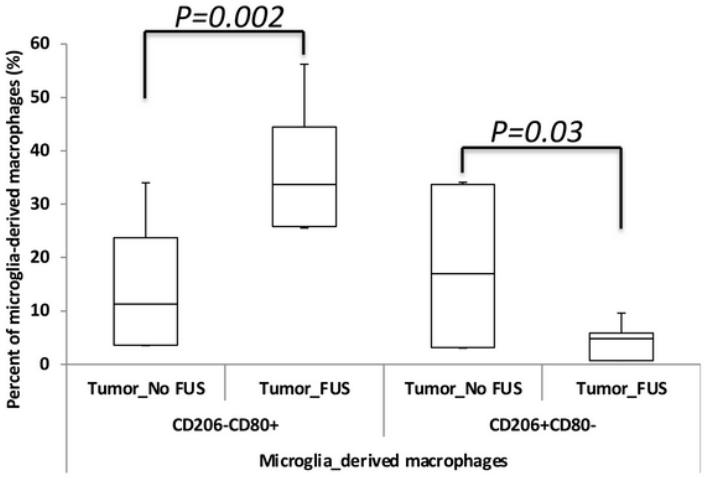

Figure 6

Effect of MRgFUS on the polarization of Tumor Associate Macrophages. The proportion of the CD80+CD206- cells in the Tumor_FUS group increased in the monocytes (p=0.04), blood-derived macrophages (p=0.005), microglia (p=0.04), and microglia-derived macrophages (p=0.002); CD80-CD206+ cells decreased in blood-derived macrophages (p=0.02) and microglia-derived macrophages (p=0.03) in Tumor_FUS group compared to Tumor_No FUS group. The proportion of CD80-CD206+ cells in Monocytes (p=0.65) and microphages (p=0.30) did not show significant difference between Tumor_No FUS and Tumor_FUS groups.

Supplementary Files

This is a list of supplementary files associated with this preprint. Click to download.

- SupplementaryFigure1.pdf
- SupplementaryFigure2.pdf